Eur. Phys. J. D **52**, 127–130 (2009)
DOI: 10.1140/epjd/e2009-00053-5

THE EUROPEAN PHYSICAL JOURNAL D

Regular Article

Structural and electronic properties of PtPd and PtNi nanoalloys

A. Radillo-Díaz, Y. Coronado, L.A. Pérez[a], and I.L. Garzón

Instituto de Física, Universidad Nacional Autónoma de México, Apartado Postal 20-364, 01000 México, D. F., México

Received 19 September 2008
Published online 18 February 2009 –

Abstract. The lowest-energy structures of binary $(PtPd)_n$, $(PtNi)_m$, $(PtNi_3)_s$, and $(Pt_3Ni)_s$ nanoclusters, with $n = 2$–28, $m = 2$–20, and $s = 4$–6, modeled by the many-body Gupta potential, were obtained by using a genetic-symbiotic algorithm. These structures were further relaxed within the density functional theory framework in order to obtain the most stable structures for each composition. Segregation is confirmed in all the $(PtPd)_n$ clusters, where the Pt atoms occupy the cluster core and the Pd atoms are situated on the cluster surface. In contrast, for the $(PtNi)_m$ nanoalloys, the Ni atoms are mainly found in the cluster core and the Pt atoms are segregated to the cluster surface. Likewise, for the $(PtNi_3)_s$ nanoalloys, Ni atoms mainly compose the cluster core but there is no clear segregation of the Pt atoms to the surface. Furthermore, for the $(Pt_3Ni)_s$ bimetallic clusters the Pt atoms concentrate in the cluster core and the Ni atoms are segregated to the surface. On the other hand, it has been experimentally found that the $Pt_{0.75}Ni_{0.25}$ supported nanoparticles present a higher catalytic activity for the selective oxidation of CO in the presence of hydrogen than the $Pt_{0.5}Ni_{0.5}$ and $Pt_{0.25}Ni_{0.75}$ nanoparticles. In order to understand this tendency in the catalytic activity, we also performed density functional calculations of the molecular CO adsorption on bimetallic Pt-Ni nanoclusters with the mentioned compositions.

PACS. 36.40.-c Atomic and molecular clusters – 36.40.Jn Reactivity of clusters – 68.43.Bc Ab initio calculations of adsorbate structure and reactions

1 Introduction

Bimetallic clusters, composed of two different metal elements, are of greater interest than monometallic ones for the improvement of catalytic properties of metal particles [1]. The great advantage of bimetallic clusters or nanoalloys is that their properties may be tuned by varying not only their size and geometries, but also their composition [2,3]. In particular, PtPd nanoparticles have been widely used as catalysts in a number of important chemical reactions involving hydrogenation such as the reduction of aromatic hydrocarbons in fuel [4]. Likewise, the PtNi alloys have important applications as electrocatalysts in low temperature polymer electrolyte fuel cells [5,6]. In the present work, the following bimetallic clusters are investigated: $(PtPd)_n$, $(PtNi)_m$, $(PtNi_3)_s$, and $(Pt_3Ni)_s$ with $n = 2$–28, $m = 2$–20, and $s = 4$–6. This study is carried out by means of density functional theory (DFT) in the generalized gradient approximation (GGA). The majority of theoretical studies of bimetallic clusters are based on the use of semiempirical many-body potentials to model the metallic bonding [3,7–10]. These potentials contain parameters that are usually obtained by fitting to experimental data of the corresponding alloy in the bulk phase, if available. They may also be obtained by averaging [7,8] or renormalizing [9] the parameters of the pure bulk metallic components. These potentials are then employed in cluster structure calculations using global optimization techniques [3,7–10] to obtain the lowest-energy isomers for a given cluster size and composition. The reliability of the resulting most stable structures of bimetallic clusters obtained with the above approach depends on the capability of the many-body potential to model the metallic bonding existing in the nanoalloy. Moreover, the lowest-energy structures of bimetallic clusters are more difficult to find than those corresponding to the pure metallic ones due to the existence of homotops, which are structural forms of a bimetallic cluster that have the same geometry, but differ by the placement of the two types of atoms at the sites of that geometry [2,3]. In the initial stage of our study, a distribution of the lowest-energy isomers of bimetallic clusters (with a given size and composition) is obtained by using the Gupta potential and a global optimization technique. In the second stage, some of the more relevant isomers of this distribution are used as initial configurations in a further local structural reoptimization, using the forces calculated from DFT-GGA. This approach has been used in previous studies of monometallic [11] and bimetallic clusters [12–14] showing an evident effectiveness. On the other hand, a given nanoalloy could have different catalytic activities for different reactions. For example, bimetallic PtNi nanoparticles supported on SiO_2 show

[a] e-mail: lperez@fisica.unam.mx

the following activity order at 300 K [15]: $Pt_{0.25}Ni_{0.75} > Pt_{0.75}Ni_{0.25} \approx Pt_{0.5}Ni_{0.5} > Pt$, for the N_2O decomposition. However, the contrary trend is observed in the case of selective oxidation of CO in the presence of hydrogen, where the $Pt_{0.75}Ni_{0.25}$ nanoparticles supported on SiO_2, present a higher catalytic activity than the nanoparticles with the other mentioned compositions [16]. In order to have some insight on the last behavior, in this work we also address the molecular CO adsorption on gas-phase Pt_mNi_n clusters with $m + n = 20$, and $m = 3n$, $m = n$ and $m = 3n$.

2 Theoretical methodology

To determine the lowest-energy structures of bimetallic clusters, we first performed global optimizations using the Gupta many-body potential [17] and a generalized version of the genetic-symbiotic algorithm by Michaelian [18,19]. The lowest-lying isomers (typically ten) of the obtained clusters, for each size and composition, were then locally reoptimized with an unconstrained conjugate gradient (CG) procedure, using the forces obtained from a DFT-GGA calculation within the PBE parametrization [20]. We used the DFT code SIESTA [21] with standard norm-conserving scalar-relativistic pseudopotentials [22] in their fully nonlocal form [23]. These pseudopotentials were generated with the atomic valence-electron configurations d^{10} (Pd), d^9s^1 (Ni and Pt), s^2p^2 (C) and s^2p^4 (O). The core radii (in atomic units) are as follows: $s(2.05)$, $p(2.05)$, $d(2.05)$ for Ni; $s(2.25)$, $p(2.25)$, $d(2.25)$ for Pd; $s(2.35)$, $p(2.50)$, $d(1.24)$ for Pt; $s(1.14)$, $p(1.14)$, $d(1.14)$ for O; and $s(1.25)$, $p(1.25)$, $d(1.25)$ for C. We used double-ζ s, d-basis and single p polarization orbitals, with maximum cutoff radii at 7.33 Å, 7.93 Å and 6.81 Å for Ni, Pd and Pt, respectively. Moreover, for C and O we used a double-ζ s, p-basis and single d orbitals. We also used an energy cutoff of 150 Ry to define the real space grid for numerical integrations. Spin polarization was not considered. All the clusters were let free to relax until the Hellmann-Feynman forces were less than 10 meV/Å. Likewise, the lowest-energy configurations of the Pt_mNi_nCO complexes were also found by performing CG structural relaxations using the DFT forces, starting with the lowest-energy isomers of the Pt_mNi_n clusters previously obtained, and testing several different initial positions (typically 20) for the adsorbed CO molecule on the bimetallic cluster. For the metal dimers the following bond distances and binding energies per atom were obtained: (2.12 Å, 1.829 eV) for Ni_2; (2.500 Å, 1.026 eV) for Pd_2; and (2.357 Å, 2.117 eV) for Pt_2. The experimental values for neutral dimers are [24]: (2.20 Å, 1.034 eV) for Ni_2; (2.48 Å, 0.698 eV) for Pd_2; and (2.34 Å, 1.855 eV) for Pt_2. It is well known the relatively high error of current xc-approximations in the calculated values of binding energies with respect to experiments. The lowest-energy isomers of $(PtPd)_n$, obtained within the DFT framework, with $n = 5$–22 and $n = 2$–20 were addressed in previous works [12,13]. For $n = 2$–4 and $n = 23$–28 we employed the method already described and the parameter set I reported in reference [7] for the Gupta potential. On the other hand, the Gupta parameters used in the global optimizations of the PtNi clusters were taken from reference [17] for Ni-Ni and Pt-Pt interactions. In the case of Pt-Ni interactions, a geometrical average of the Pt-Pt and Ni-Ni interactions was taken for the parameters A and ζ of the Gupta potential, whereas an arithmetic average was used for the parameters p, q, and r_0.

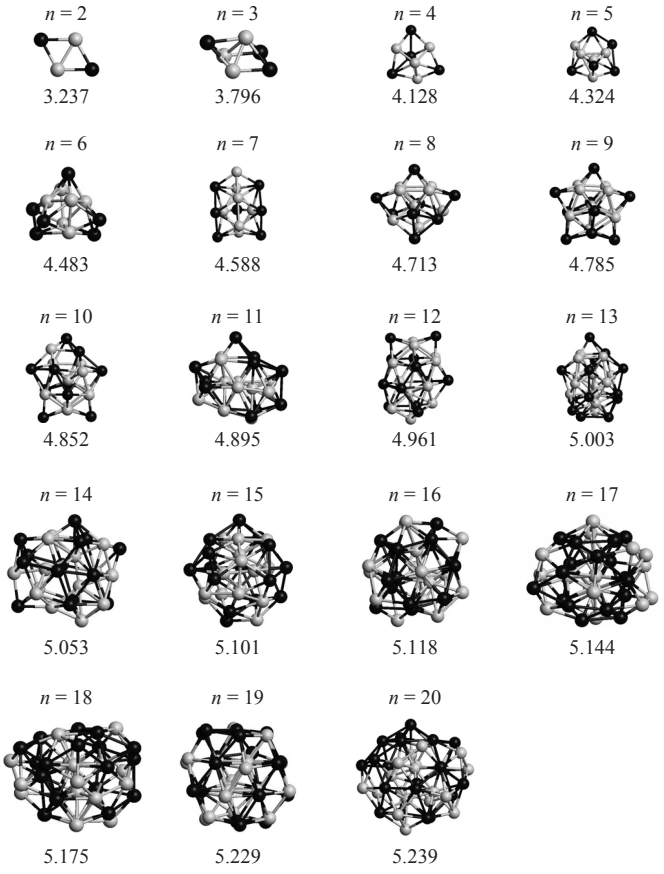

Fig. 1. Geometric structures and binding energies (in eV) for the most stable isomers of $(PtNi)_n$, with $n = 2$–20. The dark spheres represent the Pt atoms.

3 Results

The lowest-energy isomers obtained for $(PtNi)_m$, with $m = 2$–20, are shown in Figure 1. Notice that for $m = 2$, a planar structure is obtained with the Ni atoms at the center and the Pt atoms at the extremes. Almost all the structures are amorphous and some of them present decahedral ($m = 8, 10$) or icosahedral sections ($m = 13$–18, 20). For $m = 19$, the structure of the lowest-lying isomer is a distorted cube-octahedron. Interestingly, the same geometry is found for the $(PtPd)_{19}$ lowest-energy isomer. The DFT most stable isomers of $(PtPd)_n$, with $n = 5$–22, have been obtained in a previous work [12], and we have extended this study to include isomers with $n = 2$–4, and $n = 23$–28. The general trend confirmed for the $(PtPd)_n$ lowest-energy isomers is that their structure is character-

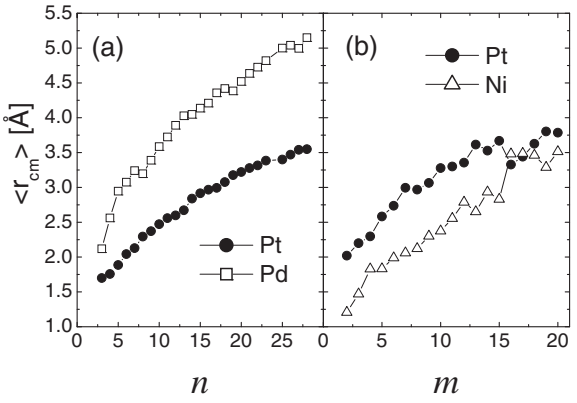

Fig. 2. Atom mean distance to cluster center of mass ($\langle r_{cm}\rangle$) versus n (m) for (a) $(PtPd)_n$ and (b) $(PtNi)_m$ with $n = 2$–28 ($m = 2$–20).

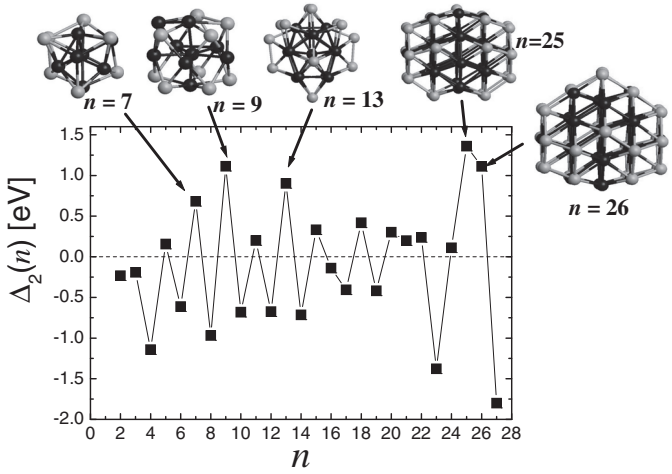

Fig. 3. Second difference in the energy [$\Delta_2(n)$] versus cluster size for $(PtPd)_n$. The dark spheres represent the Pt atoms.

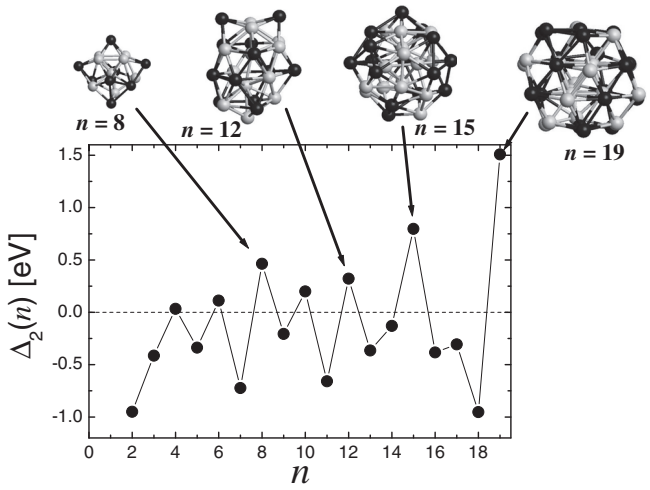

Fig. 4. Second difference in the energy [$\Delta_2(n)$] versus cluster size for $(PtNi)_n$. The dark spheres represent the Pt atoms.

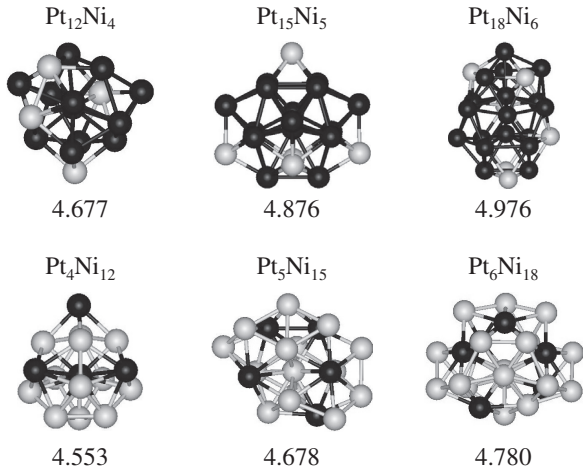

Fig. 5. Geometric structures and binding energies (in eV) for the most stable isomers of $(Pt_3Ni)_s$ and $(PtNi_3)_s$ for $s = 4$, 5, 6. The dark spheres represent the Pt atoms.

ized by a segregation phenomenon [7,8,12,13], where the Pt atoms constitute the cluster core whereas the Pd atoms are preferably on the cluster surface. This phenomenon is due to the higher binding energy of Pt atoms in comparison to that of Pd atoms, and it can be observed by inspection or by calculating the mean distance ($\langle r_{cm}\rangle$) of the atoms of each type to the cluster center of mass. In Figure 2a, $\langle r_{cm}\rangle$ is shown as a function of n for $(PtPd)_n$. Notice that the $\langle r_{cm}\rangle$ for the Pt atoms is always smaller than that corresponding to the Pd atoms for all the values of n considered. In contrast, for $(PtNi)_m$ clusters, the Pt atoms tend to segregate to the cluster surface except for $m = 16$ and 17, as shown in Figure 2b. On the other hand, an important aspect emerging from the DFT-GGA calculations is the existence of cluster sizes with special stability with respect to smaller or larger sizes. This kind of "magic number" cluster sizes can be located by calculating a second difference (Δ_2) in the cluster energy with respect to the size. For the case of bimetallic clusters with the same number n of atoms of each species, we calculated $\Delta_2(n) = E(n+1) + E(n-1) - 2E(n)$. This quantity is presented in Figure 3 for $(PtPd)_n$ clusters where the peaks at $n = 7, 9, 13, 25$ and 26 indicate a higher stability of these cluster sizes with respect to other sizes. However, this result is in contrast with that reported in reference [7], where it was found a higher stability for $n = 10, 19$ using the Gupta potential. Moreover, for $(PtNi)_n$ clusters, the lowest-energy isomers with $n = 8, 12, 15$ and 19, are more stable than the neighboring sizes (see Fig. 4).

Figure 5 shows the lowest-energy isomers of $(PtNi_3)_s$ and $(Pt_3Ni)_s$ nanoalloys, with $s = 4$–6. For the last case, the cluster core is composed by Pt atoms and the Ni atoms are segregated to the cluster surface. However, for the former case, the cluster core is composed by Ni atoms but there is no clear segregation of the Pt atoms to the cluster surface. Figure 6 shows the most stable configurations of molecular CO adsorbed on the lowest-energy Pt_mNi_n ($m+n = 20$) clusters. Table 1 shows more details of these geometries as well as the corresponding CO adsorption energies (E_{ads}), excess electronic charges (Δq) on the molecular CO and C–O bond distances. E_{ads} is calculated from $E_{ads} = E(Pt_mNi_n) + E(CO) - E(Pt_mNi_nCO)$, where $E(X)$ is the total energy of system X, and Δq is

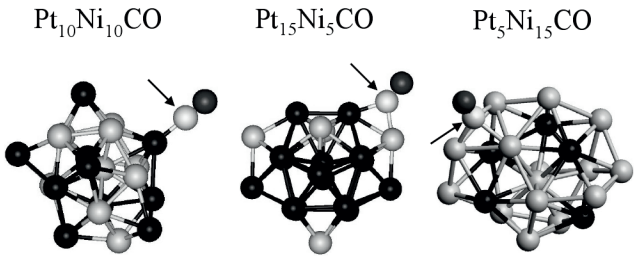

Fig. 6. Lowest-energy configurations of molecular CO adsorbed on Pt_mNi_n clusters. The dark spheres in each cluster represent the Pt atoms. For clarity, the C atom is indicated by an arrow and the dark sphere bonded to it and pointing out from the cluster represents the O atom.

Table 1. CO adsorption energies, charge transfers and C–O bond distances for Pt_mNi_nCO complexes.

	$Pt_{10}Ni_{10}CO$	$Pt_{15}Ni_5CO$	$Pt_5Ni_{15}CO$
Geometry	Top	Bridge	3-fold coord.
E_{ads} [eV]	3.117	3.528	3.252
Δq	0.084	0.172	0.248
d_{C-O} [Å]	1.19	1.21	1.23

obtained from a Mulliken population analysis. Notice that the CO always binds to the Pt_mNi_n clusters through the C atom but, depending on the cluster composition, the location of the C atom varies. For $m = n = 10$, the C atom binds to a Pt atom in a top configuration, but for $m = 15$ and $n = 5$, the C atom forms a bridge with a Pt atom and a Ni atom. Moreover, for $m = 5$ and $n = 15$, the C atom is three-fold coordinated to three Ni atoms. In all the three cases analyzed, electron transfers from the bimetallic cluster to the CO were obtained, being greater when the CO adsorbs on a three-fold coordinated position and lesser when it adsorbs on a top site. Likewise, the C–O bond distance increases with respect to the one calculated for the free CO molecule (1.17 Å) when Δq grows. Finally, the greatest adsorption energy is obtained when the CO is adsorbed onto the $Pt_{15}Ni_5$ cluster. However, the adsorption of O_2 on the Pt_mNi_n clusters should also be considered in order to have a more comprehensive understanding of the CO catalytic oxidation.

4 Summary

In this paper the structural and electronic properties of $(PtPd)_n$, $(PtNi)_m$, $(PtNi_3)_s$, and $(Pt_3Ni)_s$ nanoclusters, with $n = 2$–28, $m = 2$–20, and $s = 4$–6 were investigated within the DFT-GGA framework. The results confirm the segregation phenomenon predicted for $(PtPd)_n$ clusters where the Pt atoms are concentrated in the cluster core and the Pd atoms are situated on the cluster surface. For the $(PtNi)_n$ clusters, segregation is also found, but in this case the cluster core is mainly composed by Ni atoms whereas the Pt atoms are mainly found in the cluster surface. However, for the $(Pt_3Ni)_n$ nanoalloys, the Pt atoms concentrate in the cluster core and the Ni atoms are segregated to the surface. Moreover, for the $(PtNi_3)_n$ nanoalloys, the cluster core is constituted by Ni atoms but there is no clear segregation of the Pt atoms to the cluster surface. On the other hand, for the three Pt_mNi_nCO complexes studied, there is charge transfer from the cluster to the CO, which weakens the C–O bonding. Then, the C–O bond distance increases, being larger for the Pt_5Ni_{15} cluster where the CO binds in a 3-fold coordinated configuration with three Ni atoms, and smaller for the $(PtNi)_{10}$ cluster where the CO binds to a Pt atom in a top configuration. This configuration has the smaller adsorption energy for the CO, whereas the $Pt_{15}Ni_5CO$ complex has the greater CO adsorption energy. The calculations reported in this work are not only useful to find interesting trends in the geometries and electronic properties of bimetallic clusters, but they are also the initial step in the investigation of their catalytic properties, which could be enhanced by charge transfer effects of the type studied in this paper.

This work was supported by CONACyT under Grant 80610-F, DGAPA-UNAM under Projects IN112808 and IN113008, and the DGSCA-UNAM Supercomputing Center.

References

1. J.H. Sinfelt, *Bimetallic Catalysts: Discoveries, Concepts and Applications* (Wiley, New York, 1983)
2. J. Jellinek, E.B. Krissinel, *Theory of Atomic and Molecular Clusters*, edited by J. Jellinek (Springer, Berlin, 1999), p. 277
3. R. Ferrando, J. Jellinek, R.L. Johnston, Chem. Rev. **108**, 845 (2008)
4. V. Ponec, G.C. Bond, *Catalysis by Metals and Alloys* (Elsevier, 1995)
5. V.R. Stamenkovic et al., Science **315**, 493 (2007)
6. V.R. Stamenkovic et al., Nature Mater. **6**, 241 (2007)
7. C. Massen et al., J. Chem. Soc. Dalton Trans. **23**, 4375 (2002)
8. L.D. Lloyd, R.L. Johnston, S. Salhi, N.T. Wilson, J. Mater. Chem. **14**, 1691 (2004)
9. G. Wang et al., J. Chem. Phys. **122**, 024706 (2005)
10. A. Rapallo et al., J. Chem. Phys. **122**, 194308 (2005); G. Rossi et al., J. Chem. Phys. **122**, 194309 (2005)
11. I.L. Garzón et al., Eur. Phys. J. D **24**, 105 (2003)
12. E.M. Fernández, L.C. Balbás, L.A. Pérez, K. Michaelian, I.L. Garzón, Int. J. Mod. Phys. B **19**, 2339 (2005)
13. L.O. Paz-Borbón et al., J. Mater. Chem. **18**, 4154 (2008)
14. R. Ferrando et al., Phys. Chem. Chem. Phys. **10**, 640 (2008)
15. J. Arenas-Alatorre, A. Goméz-Cortés, M. Avalos-Borja, G. Díaz, J. Phys. Chem. B **109**, 2371 (2005)
16. J. Arenas-Alatorre, A. Goméz-Cortés, M. Avalos-Borja, G. Díaz, *13th. Int. Congress on Catalysis Proceedings* (2004), pp. 4–142
17. F. Cleri, V. Rosato, Phys. Rev. B **48**, 22 (1993)
18. K. Michaelian, Chem. Phys. Lett. **293**, 202 (1998)
19. K. Michaelian et al., Phys. Rev. B **60**, 2000 (1999)
20. J.P. Perdew et al., Phys. Rev. Lett. **77**, 3865 (1996)
21. J.M. Soler et al., J. Phys.: Cond. Mat. **14**, 2745 (2002)
22. N. Troullier, J.L. Martins, Phys. Rev. B **43**, 1993 (1991)
23. L. Kleinman, D.M. Bylander, Phys. Rev. Lett. **48**, 1425 (1982)
24. M.D. Morse, Chem. Rev. **86**, 1049 (1986)